Application of Microwave in Hydrogen Production from Methane Dry Reforming: Comparison Between the Conventional and Microwave-Assisted Catalytic Reforming on Improving the Energy Efficiency

Seyyedmajid Sharifvaghefi [1,†], Babak Shirani [1,†], Mladen Eic [1] and Ying Zheng [2,*]

[1]   Department of Chemical Engineering, University of New Brunswick, Fredericton, NB E3B 5A3, Canada
[2]   Department of Chemical and Biochemical Engineering, Thompson Engineering Building,
     Western University, London, ON N6A 5B9, Canada
*   Correspondence: ying.zheng@uwo.ca; Tel.: +1(519)661-82138
†   These authors share equal first authorship.

check for
updates

Abstract: The microwave-assisted dry reforming of methane over Ni and Ni–MgO catalysts supported on activated carbon (AC) was studied with respect to reducing reaction energy consumption. In order to optimize the reforming reaction using the microwave setup, an inclusive study was performed on the effect of operating parameters, including the type of catalysts' active metal and their concentration in the AC support, feed flow rate, and reaction temperature on the reaction conversion and H_2/CO selectivity. The methane dry reforming was also carried out using conventional heating and the results were compared to those of microwave heating. The catalysts' activity was increased under microwave heating and as a result, the feed conversion and hydrogen selectivity were enhanced in comparison to the conventional heating method. In addition, to improve the reactants' conversion and products' selectivity, the thermal analysis also clarified the crucial importance of microwave heating in enhancing the energy efficiency of the reaction compared to the conventional heating.

Keywords: dry reforming methane (DRM); methane; carbon dioxide; microwave; conversion; catalyst; selectivity; thermal integration

1. Introduction

Applying methane dry reforming process for hydrogen production has received significant attention during the last decades as a result of increasing demand for clean and renewable energy [1–5]. In addition, the main reactants of the reforming reaction, methane and carbon dioxide, have tremendous effects on global warming, which necessitate controlling their concentration by converting them to a clean and sustainable source of energy, i.e., hydrogen. In addition to hydrogen, carbon monoxide is also another valuable product of methane dry reforming reaction that is further reacted to produce ultraclean fuels including gasoline, methanol, and dimethyl ether (DME) with negligible hazardous byproducts, e.g., aromatics [6,7]. Consequently, improving the CO_2 reforming of methane is essential in terms of conversion, selectivity, and energy efficiency.

The carbon dioxide reforming of methane is an endothermic reaction, which requires huge external heat source (Equation (1)). Hence, applying novel techniques to perform the reaction with minimum input energy is necessary to improve the process efficiency and reduce the costs.

$$CH_4 + CO_2 \Leftrightarrow 2CO + 2H_2 \qquad \Delta H_{298} = 247 \text{ kJ/mol} \tag{1}$$
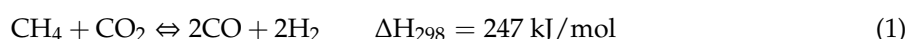
A new technique that received extensive attention in the last decades is based on using microwave energy potential for reforming of methane and carbon dioxide. In comparison to conventional heating methods, microwave applications for producing the required heat for reaction is more energy efficient and less expensive. Utilizing microwaves also provides more advantages than conventional heating including a rapid process heating, reduced processing time and work space, more accurate and uniform heating, and high quality [8–11]. In contrast, microwave heating has limitations and technical problems such as selection of the type of materials with a broad adsorption bandwidth that strongly absorb microwaves [12]. As a result, an extensive study is required on the application of microwave setup to optimize and improve the methane-reforming process in terms of conversion and product selectivity.

The dry reforming reaction takes place in the presence of a catalyst, which enhances the conversion rate, syngas selectivity, and increases the reaction rate. The applied catalysts are based on expensive noble metals (Pt, Pd, and Ru) or less expensive metals including Ni, Co, Fe, Cr, and Mo. The active metals are supported on metal oxides (Al_2O_3, MgO, and TiO_2), rare-earth oxides (CeO_2), zeolites, silicate, and mesoporous carbon materials [13–15]. In spite of the important role of catalysts on increasing the reaction rate and enhancing reactants conversion, the syngas production from methane reforming still needs to be performed at extreme conditions of high pressure and temperature [16,17]. Hence, conventional techniques have to be improved by integrating new techniques in catalytic methane reforming. The microwave heating of catalysts provides similar conversion to those of conventional heating at reduced temperatures by selective heating of active sites. In addition, the coke formation rate is smaller than conventional heating methane reforming, confirming the supremacy of microwave heating methane reforming.

In this study, carbon dioxide reforming of methane was studied in a microwave field. In order to improve adsorption efficiency of the microwaves' energy, activated carbon was used as a support for Ni and MgO active metal catalysts. Combining microwave setup and Ni-MgO/AC catalysts improved reforming reaction in terms of selectivity and conversion rates. In order to optimize the selectivity of products and conversion of reactants and the energy efficiency of the system, the effects of operating parameters such as catalyst bed temperature, feed flowrate, and also the concentration of Ni and addition of MgO were investigated in detail. The catalysts were also conventionally heated to compare the conversion, selectivity, and thermal efficiency with those obtained using microwave.

2. Results and Discussion

Textural properties, reducibility, and Ni dispersion and surface area of the prepared catalysts are shown in Table 1. With an increase in nickel content of the catalysts, the surface area and pore volume was reduced. The H_2 uptake of the catalysts, however, was found to to follow a different trend, increasing with nickel content of 15% and then being reduced for the catalysts with higher nickel content. The surface area for NiMgO/AC was found to be the lowest (539 m^2/g), however the H_2 uptake of this catalyst was only lower than the Ni/MgO/AC catalyst.

Table 1. Main characteristics of the synthesized catalysts.

	Surface Area (m^2/g)	Pore Volume (cc/g)	Average Pore Diameter (Å)	H_2 Uptake (moles/g Catalyst)	Ni Dispersion (%) [a]	Ni Surface Area (m^2/g) [a]
AC	1287	0.894	27.78	-	-	-
5Ni/AC	1004	0.733	29.20	2.80E-06	0.66	2.19
10Ni/AC	915	0.687	30.50	3.40E-06	0.40	1.33
15Ni/AC	871	0.654	31.76	4.56E-06	0.36	1.19
20Ni/AC	833	0.600	28.80	4.29E-06	0.25	0.84
25Ni/AC	665	0.473	28.46	4.16E-06	0.20	0.65
NiMgO/AC	639	0.457	28.96	5.95E-06	0.70	2.32
Ni/MgO/AC	712	0.468	26.28	6.15E-06	0.72	2.40

[a] calculated by assuming H_2/Ni atom ratio of 1.

The XRD profile of the 10Ni/AC, NiMgO/AC, and Ni/MgO/AC samples after 1 h of reduction in H_2 flow is shown in Figure 1. The peak at 26.6 can be ascribed to the AC support. The peaks at 44.4 and 76.3 are attributed to the (111) and (220) diffraction planes of Ni phase. The remaning peaks are assigned to the MgO phase. Although both NiO and MgO have the same charactristric peaks, the intensity of the peaks suggests that the NiO phase in the fresh catalyst is mostly reduced to Ni in all of the tested catalysts.
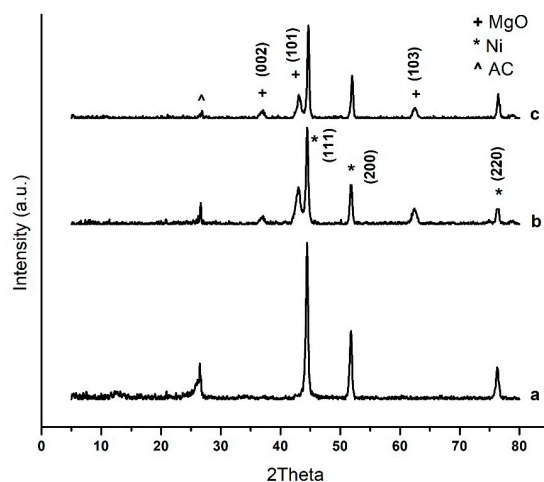

Figure 1. XRD profile of (**a**) 10Ni/AC, (**b**) NiMgO/AC, and (**c**) Ni/MgO/AC.

Temperature programmed reduction (TPR) behaviors of calcined 10Ni/AC, NiMgO/AC, and Ni/MgO/AC catalysts were investigated as shown in Figure 2. H_2 reduction for 10 Ni/AC catalyst shows the typical reduction peaks for NiO at 250 °C and 430 °C, which have been related to the reduction of Ni^{3+} and Ni^{2+} to metallic nickel, respectively [18,19]. For NiMgO/AC and Ni/MgO/AC catalysts, the first reduction peak is also observed at 250 °C, suggesting that part of the NiO phase is not influenced by the MgO. However, the second reduction peak is shifted to 740 °C, which can be assigned to the Ni^{2+} ions on the outermost layer of the MgO [20]. The wider peak for NiMgO/AC at this temperature indicates the reduction of NiO forms located in the subsurface layers of the MgO lattice, which is understandable considering that this catalyst was prepared through co-impregnation of NiO and MgO precursors. The higher dispersion of NiO in NiMgO/AC and Ni/MgO/AC facilitates the formation of smaller crystallites, which are more strongly bonded and, consequently, lowering the reducibility. On 10Ni/AC with lower dispersion, Ni species are not so strongly bonded to the surface, thus presenting a higher reducibility.
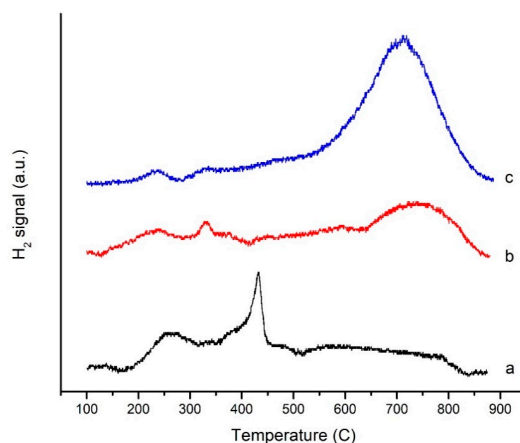

Figure 2. Temperature programmed reduction (TPR) profile of (**a**) 10Ni/AC, (**b**) NiMgO/AC, and (**c**) Ni/MgO/AC.

2.1. Temperature Effect on Conversion and Product Selectivity

The conversions of CH_4 and CO_2 over the synthesized catalysts at different temperatures using microwave as the heating medium, are shown in Figure 3a,b, respectively. It can be seen that the increase in temperature of reaction accelerates the reforming reaction resulting in higher conversion of the reactants at higher temperatures. As evidenced, among the Ni/AC catalysts, 15% nickel loading shows the highest conversion with 76% and 79% for CH_4 and CO_2, respectively. Conversions follow a decreasing trend with higher nickel content. The observed trend can be related to the H_2 uptake and nickel dispersion results by these catalysts, which shows the same trend. The results indicate that with the increase in nickel content up to 15% the number of available sites for the adsorption of the reacting gases was increased. However, with the addition of extra nickel to the catalyst, the nickel particles agglomerate and, therefore, the dispersion of the catalyst was reduced, resulting in lower active sites and lower conversion of the reactants.
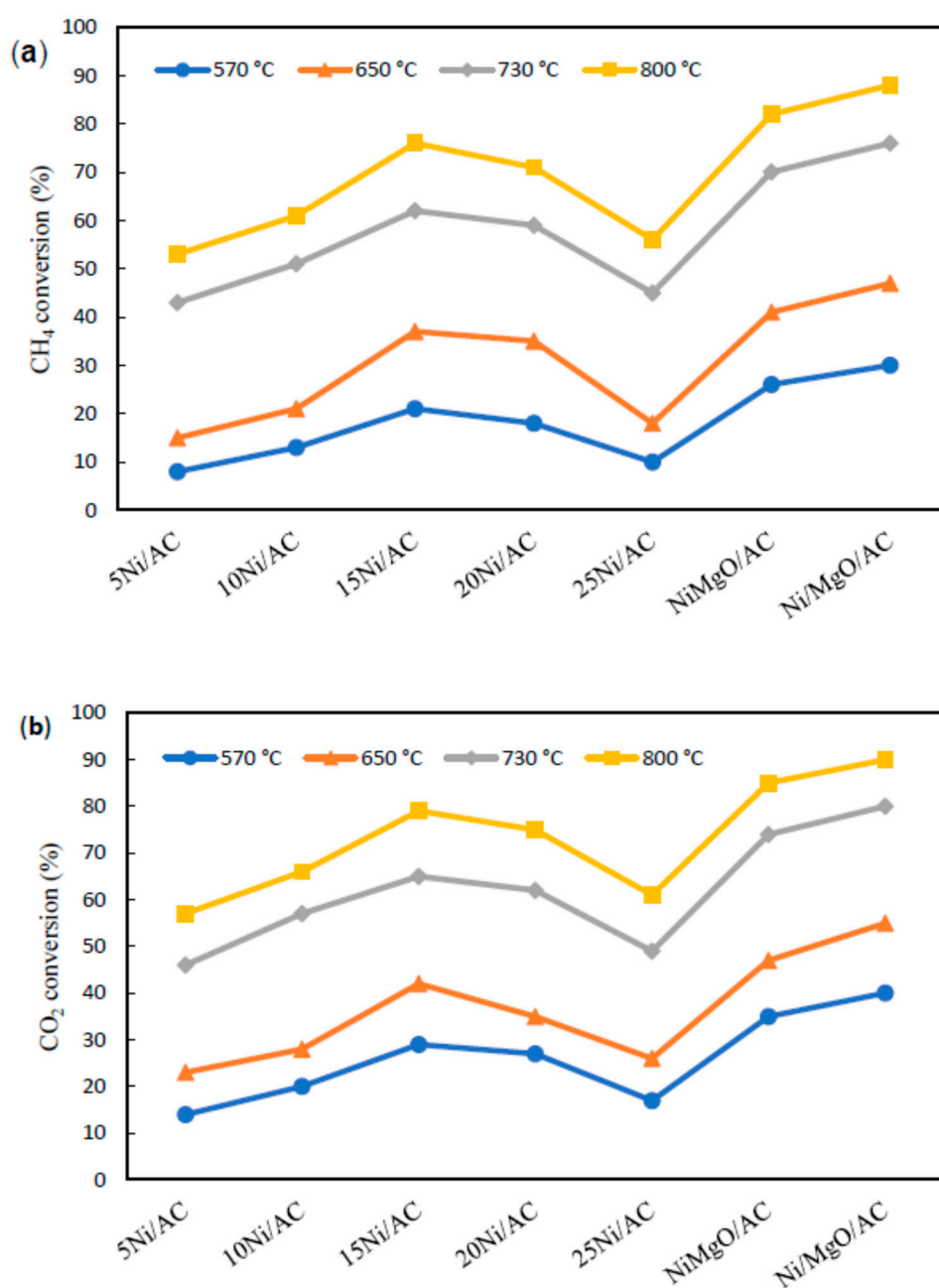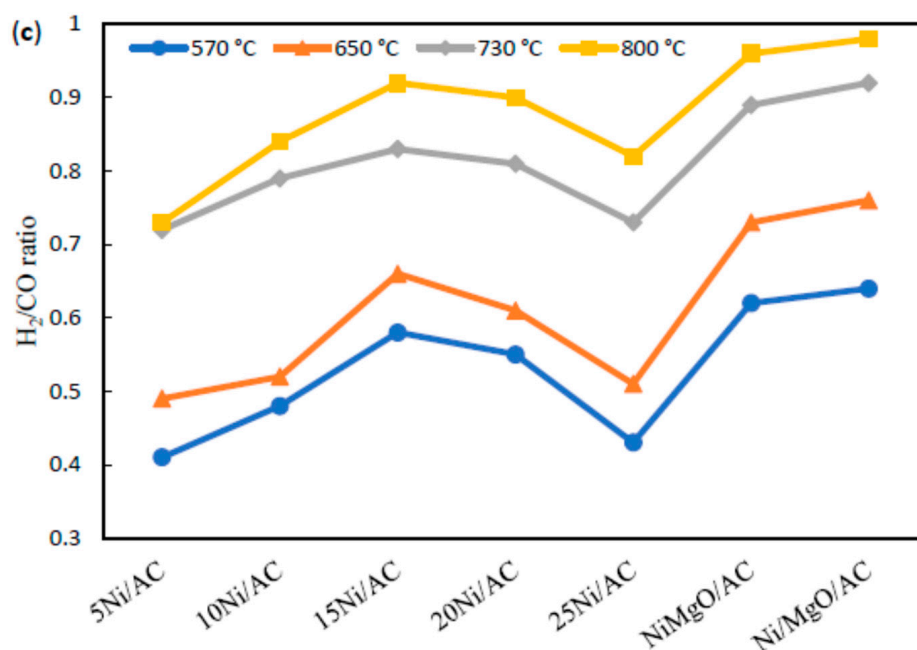

Figure 3. *Cont.*

Figure 3. (**a**) CO_2 and (**b**) CH_4 conversions and (**c**) product selectivity as a function of temperature over the prepared catalysts using microwave heating.

The results show that the conversion of CH_4 and CO_2 increases almost linearly with nickel content of the catalysts (up to 15%). Furthermore, the addition of MgO to the catalyst was found to have a positive impact on the activity of the catalysts increasing the CH_4 conversion to 84% and 88% for NiMgO/AC and Ni/MgO/AC catalysts. H_2 uptake and dispersion results for these catalysts suggest that with the addition of MgO, nickel dispersion over the AC support is enhanced and therefore the number of active sites for the reforming reactions is increased. Comparing NiMgO/AC with Ni/MgO/AC, the conversion for the later catalyst was found to be higher. This could be attributed to the fact that with co-impregnation of NiO and MgO, parts of the NiO phase will be located beneath the MgO layers making them inaccessible to the reacting gases. Figure 3c shows the H_2/CO ratio for the tested catalysts at various temperatures. The products ratio follows the same trend as the conversion of the reactants for the catalysts. Moreover, with temperature increase, the ratio was increased for all the catalysts.

2.2. Effect of Heating Mechanism on Methane Reforming

To study the effect of the microwave heating on the dry reforming reaction, the experiments were also carried out using conventional heating over Ni/MgO/AC catalyst. The results are shown in Figure 4. The equilibrium conversions of CO_2 and CH_4 and the equilibrium molar ratio of H_2/CO are also plotted in the Figure 4. Two reactions were considered to perform the equilibrium calculations, i.e., methane reforming by carbon dioxide and reverse water–gas shift reaction (RWGS). It is believed that the reforming of methane starts by decomposition of CH_4 to carbonaceous deposits (Equation (2)). These deposits (at least those which are highly reactive), are gasified in the next step by CO_2 (Equation (3)), giving rise to an in-situ regeneration of the active sites. The reverse water–gas shift reaction also occurs as a side reaction in which some of the H_2 from the CH_4 decomposition reacts with the CO_2 to produce H_2O and CO (Equation (4)). The equilibrium data were obtained from the thermodynamic analysis of the results.
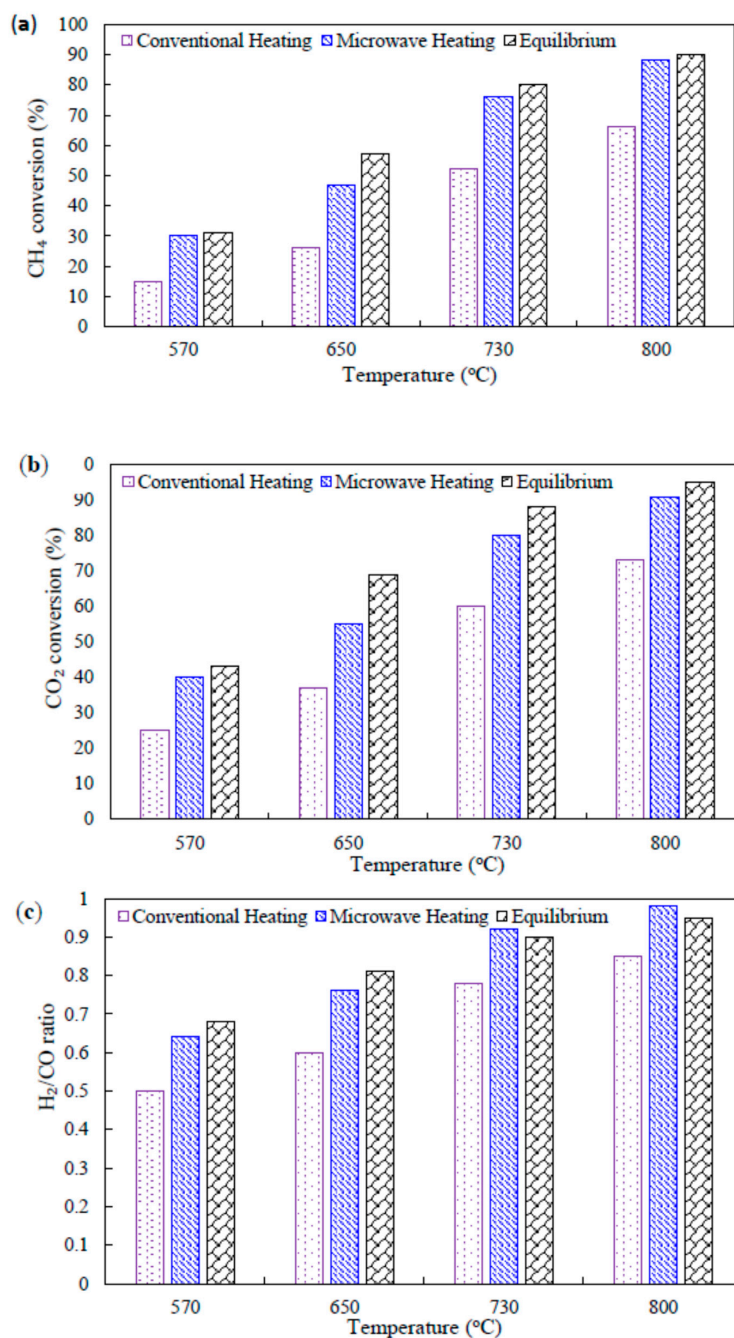
$$CH_4 \rightarrow C + 2H_2 \tag{2}$$

$$C + CO_2 \rightarrow 2CO \tag{3}$$

$$CO_2 + H_2 \Leftrightarrow H_2O + CO \tag{4}$$

Figure 4. Comparison of microwave and conventional heating and equilibrium conditions for (**a**) CO_2 and (**b**) CH_4 conversions and (**c**) product selectivity as a function of temperature over Ni/MgO/AC catalyst and gas hourly space velocity (GHSV) of 33,000 mL/g cat.h.

Compared to the conventional heating, the conversion of methane and carbon dioxide were both higher using microwave heating. The difference in conversions can be explained by the differences between the heating mechanisms. In conventional heating, heat flux is responsible for energy transfer while microwave energy is directly transferred to the catalyst, without any heat flux. This results in higher temperature inside the catalyst compared to the temperature of the surrounding atmosphere near the surface, which can be translated to higher uniformity of heat distribution with respect to conventional heating [21,22]. Microwave heating also gives rise to micro-plasmas (also called hot spots) within the catalyst bed, where the temperature is higher than the measured average temperature in the bulk catalyst bed [23]. Such hot spots with higher temperature are reported to be responsible

for enhancements in reaction rate, higher yields, and improved selectivity of heterogeneous catalytic reactions [24–26]. It is interesting to note that the conversions of CO_2 and CH_4 were always higher under microwave conditions with an almost constant difference with conventional heating. In contrast to conventional heating, microwave heating can generate multiple hot spots at the catalyst surface, where local reaction temperatures are higher than the overall reaction temperature.

In general, the results show that the H_2/CO ratios increased when the temperature was raised. With conventional heating, the H_2/CO ratio was lower than the equilibrium values. In contrast, the H_2/CO ratio was higher than the equilibrium value in the higher temperature range under microwave heating. The H_2/CO ratio was always found to be less than 1.0, an indication that the reverse water–gas shift reaction also occurred as a side reaction in addition to the methane reforming reaction. The variation of H_2/CO ratios depends on the degree of competition between these reactions. Based on the thermodynamic data, both the CH_4 reforming and the reverse water–gas shift reactions are endothermic. By increasing the temperature, both equilibrium constants (K_p) increased, but the enhancement of K_P for the CH_4 reforming reaction was to a greater extent than that for the reverse water–gas shift reaction. This showed higher impact of temperature on the first reaction to produce hydrogen and carbon monoxide, giving a ratio closer to unity. The higher H_2/CO ratio for microwave system can be explained by the creation of hot spots, which is similar to that from the thermal temperature effect. Using microwave heating, the reaction could occur at a higher temperature compared to the measured average temperature, so a higher H_2/CO ratio could be reached, which can be even higher than the equilibrium value at the measured temperature.

2.3. Effect of Varying Flow Rate on Methane Reforming

The effect of varying the flow rate on the conversion of CH_4 and CO_2 at 650 °C for Ni/MgO/AC catalyst is shown in Figure 5. CH_4 conversion decreased from 89% to 47% when gas hourly space velocity (GHSV) varies from 6700 mL/g cat.h to 33,000 mL/g cat.h. The results show a linear relation between the conversion of reactants and the flow rate of the inlet gases. The larger the GHSV, the lesser the contact time and the number of adsorbed reactants on the active sites. Unlike the results shown in Figure 4 where conversions of CO_2 and CH_4 were below equilibrium for GHSV of 33,000 mL/g cat.h, the reduction in flow rate leads to higher conversions than the calculated equilibrium. This shift in equilibrium for the methane reaction is also an indication of the presence of higher temperature at reacting sites (hot spots) than the measured average temperature of the bulk catalyst. With the decrease in GHSV, the H_2/CO ratio was increased. This can be attributed to the increase in gas–solid contact time. With higher contact time, the water–gas shift reaction can occur to consume the produced CO and therefore increase the H_2/CO ratio.
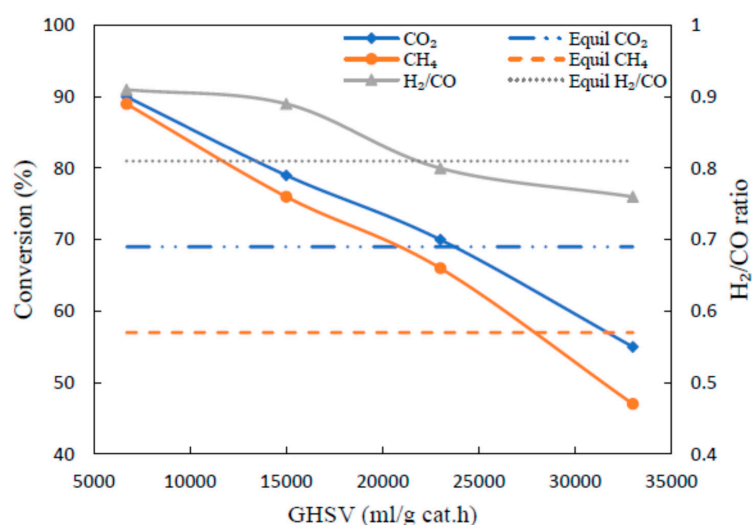

Figure 5. Effect of GHSV on Ni/MgO/AC catalyst performance for dry reforming of methane at 650 °C.

2.4. Reactor Energy Efficiency

Following the analysis presented by Durka et al. [27], an energy balance in macroscopic level is performed over the catalytic bed as follows:

$$\sum_i n_{i_{In}} \int_{T_{amb}}^{T_{in}} C_{p_i}(T)dT + Q_{Input} - Q_{Loss} = \Delta H_r^{T_{amb}} + \sum_i n_{out} \int_{T_{amb}}^{T_{out}} C_{p_i}(T)dT \tag{5}$$

where n_i is the number of moles of reactants and products, T_{amb} is the ambient temperature, T_{in} and T_{out} are the temperature of preheated reactants and products respectively, Q_{Input} is the heat provided to the reactor bed from the energy source, and Q_{Loss} is the heat dissipated to the surrounding. Since summation of the terms in left side of Equation (5) represents the net input energy into the reactor, Durka et al. [27] defined the energy efficiency as the fraction of input heat required to taking place the chemical reaction:

$$\epsilon = \frac{\Delta H_r^{T_{amb}}}{\Delta H_r^{T_{amb}} + \sum_i n_{out} \int_{T_{amb}}^{T_{out}} C_{p_i}(T)dT} \tag{6}$$

where ϵ is the energy efficiency. In the present study, in addition to the reaction between methane and carbon dioxide, reaction 4 is also considered as the side reaction. By considering the carbon dioxide as the limiting reactant, the total heat released from Equations (1) and (4) at ambient temperature is calculated based on the total mole of reacted CO_2. The results of the energy analysis for microwave and conventional heating reactor using 10Ni/AC and Ni/Mgo/AC catalysts are shown in Figure 6.
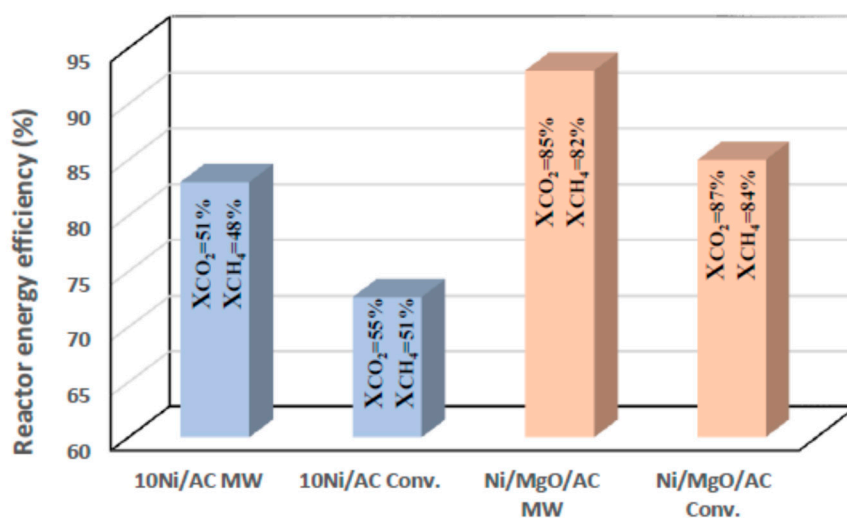

Figure 6. Energy efficiencies of microwave and conventional heating reactors using Ni/AC and Ni/MgO/AC catalysts.

According to Figure 6, similar conversions of carbon dioxide and methane were selected to compare the energy efficiency of the two reactors. As a result, the heat of reaction is constant for both microwave and conventional heating technique and the only factor determining the reactor efficiency is the heat dissipating out of the reactor with the product (Equation (6)). The catalyst bed in the microwave reactor has a lower temperature than the one in the conventional heating reactor at equal conversion. The temperatures of the bed and product gases for microwave and conventional heating reactors applying 10Ni/AC and Ni/MgO/AC catalysts are summarized in Table 2. The results indicate that applying microwave for heating the catalysts results in lower overall reaction temperature at similar conversion. The reason is because of the significant temperature difference between the metal sites and support materials [27]. This temperature difference results in significantly higher temperature metal reaction sites than the support and gas phase, providing similar conversion to conventional

reactor. The product temperature leaving the microwave reactor has a significantly lower temperature than those leaving the conventionally heated reactor. Consequently, based on Equation (6), the energy efficiency of the microwave reactor is greater than the conventional reactor. According to Figure 6, applying microwave heating resulted in 10% improvement in energy efficiency for the bed filled with 10Ni/AC catalyst and 8% for the bed of Ni/MgO/AC catalyst.

Table 2. Temperatures of the beds and product gases for microwave and conventional heating reactors.

Catalyst	T_{Bed} (°C)	$T_{outlet-gas}$ (°C)
10Ni/AC MW	690	216
10Ni/AC Conv.	900	571
Ni/MgO/AC MW	695	212
Ni/MgO/AC Conv.	900	560

Based on the results, it is clear that the microwave performs the reaction at a considerably lower temperature, and it is more energy efficient. However, it should be emphasized that the greater energy efficiency values do not necessarily means that the total energy required by microwave is less than the conventional heating reactors. Precise analysis on magnetron efficiencies and the energy loss in microwave conversion to heat has to be carried out to optimize the consumed energy by the microwave. Another advantage of applying the microwave in providing the reaction energy is the fast stabilization of the bed temperature. In comparison to conventional heating, where a few hours were required for the bed approaching the reaction temperature, the microwave heated the bed in a significantly shorter time and the reaction temperature was reached in a few minutes.

3. Experimental

3.1. Catalyst Preparation and Characterization

The xNi/AC with different Ni metal loading (x showing the Ni loading) were prepared by incipient wet impregnation. To prepare the xNi/AC, an aqueous solution containing the required mass of $Ni(NO_3)_2.6H_2O$ (Sigma-Aldrich) was added to AC support (from Carbon Resources, coal based HCL washed) to make 5, 10, 15, 20, and 25Ni/AC. 10Ni/10MgO/AC (named Ni/MgO/AC herein) and 10Ni-10MgO/AC (named NiMgO/AC herein) catalysts were also prepared using the impregnation technique. The Ni/MgO/AC catalyst was synthesized by step-wise impregnation of first the MgO precursor ($Mg(NO_3)_2.6H_2O$, Sigma-Aldrich) followed by drying and calcination and then the addition of Ni precursor. NiMgO/AC catalyst was prepared by co-impregnation of the MgO and Ni precursors. The catalysts were dried under continuous stirring at 90 °C followed by drying at 120 °C for 24 h. The catalysts were eventually calcined at 700 °C with a ramp rate of 10 °C/min under Argon stream for 5 h. The catalysts were reduced at 600 °C prior to their characterization. The textural properties of the prepared catalysts including BET surface area, pore volume, and pore diameter were measured by analyzing nitrogen adsorption–desorption isotherm at 77 K using Autosorb-1 (Quantachrome Instrument). In addition, the crystalline patterns of the catalysts were determined by X-ray diffraction (XRD) using a Bruker D8 Advance spectrometer. The diffractometer was equipped with a two-circle goniometer housed in a radiation safety enclosure. The X-ray source was a sealed, 2.2 kW Cu X-ray tube (X-ray wavelength 1.54 A), maintained at an operating current of 40 kV and 25 mA. Samples were scanned in the range of 10–80° 2θ. A step size of 0.02° and a step time of 1.0 s were used during the measurements. A peltier-cooled solid-state [Si(Li)] detector (Sol-X) with a useful energy range of 1 to 60 KeV was used as the detector.

The hydrogen temperature programmed reduction (TPR) analysis for fresh catalysts were performed using Autosorb-1. For TPR analysis, about 10 mg catalyst was regenerated in helium flow for 2 h at 120 °C. After removing the moistures, a helium stream that contained 5% hydrogen was introduced to the catalyst, and the system was heated up to 1000 °C with a heating rate of 10 °C/min

to reduce the catalysts. The data regarding the temperature were collected using a thermocouple placed in a catalyst bed for accurate measurement. H_2 chemisorption was performed to determine the nickel dispersion and nickel surface area. Further, 10 mg of catalyst was first reduced in-situ at 600 °C. The catalyst was subsequently purged with Ar flow at 600 °C and was then cooled down to room temperature. Hydrogen was introduced again as a mixture of H_2 (2%) and Ar (98%) with total flow rate of 50 mL/min. The catalyst was flushed with argon at 80 °C and the temperature was raised afterwards with only argon flowing. The effluent gas from the catalyst bed was analyzed by mass spectroscopy (RGA 200, SRS) to determine the H_2 concentration. Nickel dispersion and surface area were calculated considering the one-on-one adsorption of hydrogen on nickel atoms and atomic nickel cross-sectional area of 6.49×10^{-20} m^2/Ni-atom by the following equations:

$$\text{Dispersion} = \text{S. M. N/100W} \tag{7}$$

$$\text{Surface Area} = \text{N. L. C/100W} \tag{8}$$

where S is a stoichiometric factor. That means, for example, in the case of Ni and H_2 chemisorption, one molecule of H_2 dissociates to give two atoms to be chemisorbed on Ni atoms. N is the amount of monolayer, experimentally obtained from flow experiments in mol/g cat. M is the molecular weight of the metal (g/mol). W is the weight percentage of metal. L is the Avogadro number and C is the nickel cross-sectional area (m^2/Ni-atom).

3.2. Experimental Setup

Microwave Setup: The schematic diagram of the microwave setup is shown in Figure 7. The dry reforming reaction was carried out in a fixed-bed quartz tube with an inside diameter of 16.9 mm and a length of 9.2 mm. The catalysts (0.9 g) were placed in the waveguide channel and were heated by microwaves reaching the reaction temperature. The quartz wool was used to adjust the location of catalyst bed in the center of waveguide channel. The temperature of the catalyst bed was measured using a thermo-gun (model Milwakee M12) through an open window in front of the catalyst. The thermo-gun was calibrated before the experiments. The system was at atmospheric pressure and the applied microwave power was set to change the temperature of the catalyst. Prior to the catalytic reaction, the catalyst was reduced at 600 °C for 2 h with hydrogen flow of 50 mL/min. After heating the catalysts to the reaction temperature, a mixture of methane-carbon dioxide (1:1) with a total flowrate of 500 mL/min was heated in an electric pre-furnace, which contained a 15 m circular 1/8″ stainless-steel tube, for preheating, and eventually fed to the catalyst bed. About 30 min after feed introduction, when the products' concentration became stable, the gas products were sampled and analyzed using a gas chromatograph (GC, Varian 3400) equipped with a residual gas analyzer (RGA 200). The product sampling was repeated three times and reasonable accuracy (less than 1% difference) in the results was obtained.

Conventional Heating Setup: Similar setup to microwave was used with a difference that in these set of experiments; a quartz tubular U-shaped reactor was used to hold 0.9 g of catalyst. The reactor had a diameter (i.d.) of 7.9 mm and a length of 36.3 mm for holding catalysts. The reactor was heated in a furnace and the bed temperature was measured using a type R thermocouple placed inside the tube in the furnace. Similar operating conditions to that of the catalytic-microwave reaction was applied, and the effects of temperature and metal content were investigated and compared to the results from microwave setup.

Data Evaluation: The methane and carbon dioxide conversions and hydrogen and carbon monoxide selectivities were calculated using the following equations:

$$X_{CH_4} = \frac{n_{T,in} \times y_{CH4,in} - n_{T,out} \times y_{CH4,out}}{n_{T,in} \times y_{CH4,in}} \times 100 \tag{9}$$

$$X_{CO_2} = \frac{n_{T,in} \times y_{CO2,in} - n_{T,out} \times y_{CO2,out}}{n_{T,in} \times y_{CO2,in}} \times 100 \tag{10}$$

$$S_{H_2} = \frac{n_{T,out} \times y_{H2,out}}{n_{T,in} - (n_{T,out} \times y_{CH4,out} + n_{T,out} \times y_{CO2,out})} \times 100 \tag{11}$$

$$S_{CO} = \frac{n_{T,out} \times y_{CO,out}}{n_{T,in} - (n_{T,out} \times y_{CH4,out} + n_{T,out} \times y_{CO2,out})} \times 100 \tag{12}$$

$$R_{H2/CO} = \frac{n_{T,out} \times y_{H2,out}}{n_{T,out} \times y_{CO,out}} \tag{13}$$

where X is the conversion, S is the selectivity, y is the mole fraction, $n_{T,in}$ is the total moles of the input gases, and $n_{T,out}$ is the total moles of output gases.
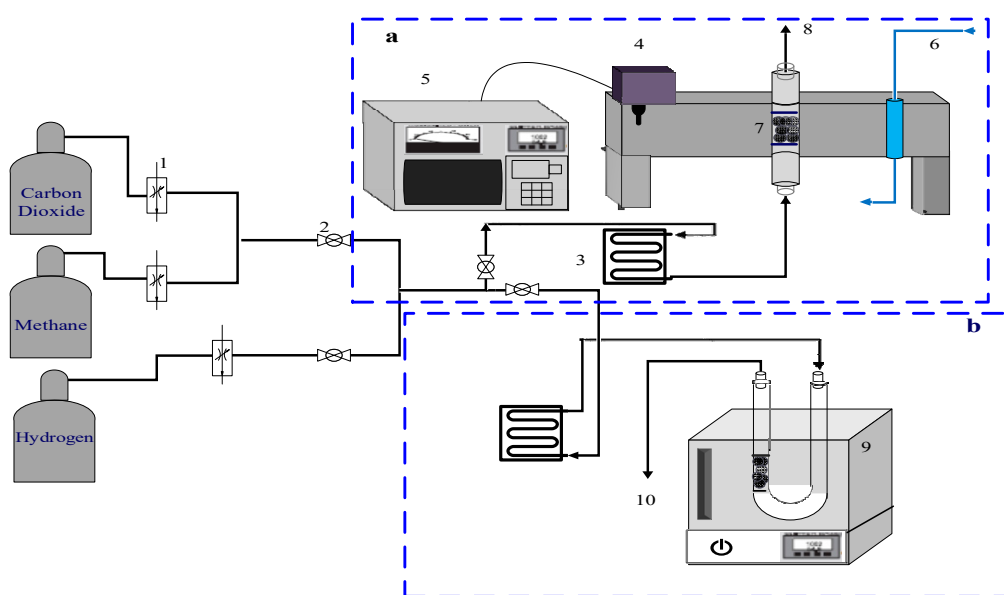
Figure 7. Schematic diagram of (**a**) microwave and (**b**) conventional setups for methane dry reforming. (1) Mass flow controller. (2) Ball valve. (3) Preheater jacket. (4) Microwave magnetron (5) Microwave power supply. (6) Cooling water. (7) Catalyst bed (quartz tube). (8) Products from microwave reactor. (9) Furnace. (10) Product from conventional reactor.

The equilibrium constant is given in terms of mole fractions y or number of moles n of the individual components for both methane reforming (MR) and reverse water gas shift (RWGS) reactions as follows:

$$k_{MR} = \frac{p_{H_2}^2 \cdot p_{CO}^2}{p_{CO_2} \cdot p_{CH_4}} = \frac{y_{H_2}^2 \cdot y_{CO}^2}{y_{CO_2} \cdot y_{CH_4}} \cdot P_{Tot}^2 = \frac{n_{H_2}^2 \cdot n_{CO}^2}{n_{CO_2} \cdot n_{CH_4} \cdot n_{Tot}^2} \cdot P_{Tot}^2 = \exp(-\Delta G_{MR}/RT) \tag{14}$$

$$k_{RWGS} = \frac{y_{H_2O} \cdot y_{CO}}{y_{CO_2} \cdot y_{H_2}} = \frac{n_{H_2O} \cdot n_{CO}}{n_{CO_2} \cdot n_{H_2}} = \exp(-\Delta G_{RWGS}/RT). \tag{15}$$

In order to calculate the equilibrium conversions, the equilibrium constant was calculated by finding the Gibbs free energy. The calculations were performed using MATLAB.

4. Conclusions

Methane reforming by CO_2 was investigated in this study over series of Ni/AC, NiMgO/AC, and Ni/MgO/AC catalysts using microwave as the heating source. Among Ni/AC catalysts with varying nickel loading, 15Ni/AC showed the highest activity. The addition of Mg as the promoter was found to enhance the activity of the catalyst by increasing nickel dispersion. H_2/CO ratio was also

increased, indicating that with the addition of Mg, the effect of secondary reaction was less profound. Increasing the reaction temperature was found to improve the conversion of reactants, which was expected as the reforming reaction is endothermic. Increasing the temperature from 650 °C to 730 °C showed the highest increase in conversion and H_2/CO ratio.

Compared to conventional heating, applying microwave heating at the same catalyst bed temperature for both heating systems resulted in significant enhancement of the methane conversion. However, for high flow rate (GHSV of 33,000 mL/g cat.h), the conversions were below the equilibrium value. Decreasing the flow rate, the conversions passed the equilibrium values for the tested temperature (650 °C). The higher conversions were related to the creation of micro-plasmas or hot spots over the active sites increasing the reaction temperature higher than the measured average temperature of catalyst bed.

Reactor energy efficiency based on the outlet gas temperatures was compared between both heating mechanisms for 10Ni/AC and Ni/MgO/AC catalysts. The microwave heating was found to have lower outlet gas temperature and higher efficiency than its conventional counterpart.

References

1. Wysocka, I.; Hupka, J.; Rogala, A. Catalytic Activity of Nickel and Ruthenium–Nickel Catalysts Supported on SiO_2, ZrO_2, Al_2O_3, and $MgAl_2O_4$ in a Dry Reforming Process. *Catalysts* **2019**, *9*, 540. [CrossRef]

2. Chun, S.M.; Shin, D.H.; Ma, S.H.; Yang, G.W.; Hong, Y.C. CO_2 Microwave Plasma—Catalytic Reactor for Efficient Reforming of Methane to Syngas. *Catalysts* **2019**, *9*, 292. [CrossRef]

3. Kumar, A. Low Temperature Activation of Carbon Dioxide by Ammonia in Methane Dry Reforming—A Thermodynamic Study. *Catalysts* **2018**, *8*, 481. [CrossRef]

4. Chung, W.C.; Chang, M.B. Dry reforming of methane by combined spark discharge with a ferroelectric. *Energy Convers. Manag.* **2016**, *124*, 305–314. [CrossRef]

5. Hamzehlouia, S.; Jaffer, S.A.; Chaouki, J. Microwave Heating-Assisted Catalytic Dry Reforming of Methane to Syngas. *Sci. Rep.* **2018**, *8*, 8940. [CrossRef] [PubMed]

6. Choudhary, T.V.; Choudhary, V.R. Energy-Efficient Syngas Production through Catalytic Oxy-Methane Reforming Reactions. *Angew. Chem. Int. Ed.* **2008**, *47*, 1828–1847. [CrossRef] [PubMed]

7. Abdullah, A.Z.; Bhatia, S.; Fan, M.-S.; Fan, M. Catalytic Technology for Carbon Dioxide Reforming of Methane to Synthesis Gas. *ChemCatChem* **2009**, *1*, 192–208.

8. Caddick, S.; Fitzmaurice, R.; Li, H.; Nguyen, N.; Fronczek, F.R.; Vicente, M.G.H. Microwave enhanced synthesis. *Tetrahedron* **2009**, *65*, 3315–3323. [CrossRef]

9. Ku, H.; Siores, E.; Taube, A.; Ball, J. Productivity improvement through the use of industrial microwave technologies. *Comput. Ind. Eng.* **2002**, *42*, 281–290. [CrossRef]

10. De la Hoz, A.; Diaz-Ortiz, A.; Moreno, A. Microwaves in organic synthesis. Thermal and non-thermal microwave effects. *Chem. Soc. Rev.* **2005**, *34*, 164–178. [CrossRef]

11. Gude, V.; Patil, P.; Martinez-Guerra, E.; Deng, S.; Nirmalakhandan, N. Microwave energy potential for biodiesel production. *Sustain. Chem. Process.* **2013**, *1*, 5. [CrossRef]

12. Xiong, L.; Yu, M.; Liu, J.; Li, S.; Xue, B. Preparation and evaluation of the microwave absorption properties of template-free graphene foam-supported Ni nanoparticles. *RSC Adv.* **2017**, *7*, 14733–14741. [CrossRef]

13. Yang, Y.C.; Lee, B.J.; Chun, Y.N. Characteristics of methane reforming using gliding arc reactor. *Energy* **2009**, *34*, 172–177. [CrossRef]

14. Heintze, M.; Pietruszka, B. Plasma catalytic conversion of methane into syngas: The combined effect of discharge activation and catalysis. *Catal. Today* **2004**, *89*, 21–25. [CrossRef]

15. Wang, Y.F.; Tsai, C.H.; Chang, W.Y.; Kuo, Y.M. Methane steam reforming for producing hydrogen in an atmospheric-pressure microwave plasma reactor. *Int. J. Hydrogen Energy* **2010**, *35*, 135–140. [CrossRef]

16. Zeng, Y.; Zhu, X.; Mei, D.; Ashford, B.; Tu, X. Plasma-catalytic dry reforming of methane over γ-Al$_2$O$_3$ supported metal catalysts. *Catal. Today* **2015**, *256*, 80–87. [CrossRef]

17. Kraus, M.; Egli, W.; Haffner, K.; Eliasson, B.; Kogelschatz, U.; Wokaun, A. Investigation of mechanistic aspects of the catalytic CO$_2$ reforming of methane in a dielectric-barrier discharge using optical emission spectroscopy and kinetic modeling. *Phys. Chem. Chem. Phys.* **2002**, *4*, 668–675. [CrossRef]

18. Kalai, D.Y.; Stangeland, K.; Jin, Y.; Tucho, W.M.; Yu, Z. Biogas dry reforming for syngas production on La promoted hydrotalcite-derived Ni catalysts. *Int. J. Hydrogen Energy* **2018**, *43*, 19438–19450. [CrossRef]

19. Solsona, B.; Concepción, P.; Nieto, J.M.L.; Dejoz, A.; Cecilia, J.A.; Agouram, S.; Soriano, M.D.; Torres, V.; Jiménez-Jiménez, J.; Castellón, E.R. Nickel oxide supported on porous clay heterostructures as selective catalysts for the oxidative dehydrogenation of ethane. *Catal. Sci. Technol.* **2016**, *6*, 3419–3429. [CrossRef]

20. Parmaliana, A.; Arena, F.; Frusteri, F.; Giordano, N. Temperature-programmed reduction study of NiO?MgO interactions in magnesia-supported Ni catalysts and NiO?MgO physical mixture. *J. Chem. Soc. Faraday Trans.* **1990**, *86*, 2663. [CrossRef]

21. Zlotorzynski, A. The Application of Microwave Radiation to Analytical and Environmental Chemistry. *Crit. Rev. Anal. Chem.* **1995**, *25*, 43–76. [CrossRef]

22. Meredith, R.J. *Engineers' Handbook of Industrial Microwave Heating, Iet*; The Institution of Electrical Engineers: London, UK, 1998.

23. Domínguez, A.; Fernández, Y.; Fidalgo, B.; Pis, J.; Menéndez, J. Biogas to syngas by microwave-assisted dry reforming in the presence of char. *Energy Fuels* **2007**, *21*, 2066–2071. [CrossRef]

24. Stuerga, D.; Gaillard, P. Microwave heating as a new way to induce localized enhancements of reaction rate. Non-isothermal and heterogeneous kinetics. *Tetrahedron* **1996**, *52*, 5505–5510. [CrossRef]

25. Will, H.; Scholz, P.; Ondruschka, B. Heterogeneous Gas-Phase Catalysis Under Microwave Irradiation—A New Multi-Mode Microwave Applicator. *Top. Catal.* **2004**, *29*, 175–182. [CrossRef]

26. Zhang, X.; Hayward, D.O.; Mingos, D.M.P. Effects of Microwave Dielectric Heating on Heterogeneous Catalysis. *Catal. Lett.* **2003**, *88*, 33–38. [CrossRef]

27. Durka, T.; Stefanidis, G.D.; Van Gerven, T.; Stankiewicz, A.I. Microwave-activated methanol steam reforming for hydrogen production. *Int. J. Hydrogen Energy* **2011**, *36*, 12843–12852. [CrossRef]